Myoplasmic resting Ca2+ regulation by ryanodine receptors is under the control of a novel Ca2+-binding region of the receptor

Biochem. J. (2014) **460**, 261–271 (Printed in Great Britain) doi:10.1042/BJ20131553

Myoplasmic resting Ca^{2+} regulation by ryanodine receptors is under the control of a novel Ca^{2+}-binding region of the receptor

Yanyi CHEN*[1], Shenghui XUE*[1], Juan ZOU*, Jose R. LOPEZ†, Jenny J. YANG*[2] and Claudio F. PEREZ‡[2]

*Department of Chemistry, Center for Diagnostics and Therapeutics, Georgia State University, 50 Decatur Street, NSC 552, Atlanta, GA 30303, U.S.A.
†Department of Molecular Biosciences, School of Veterinary Medicine, University of California, Davis, 1089 Veterinary Medicine Drive, Davis, CA 95616, U.S.A.
‡Department of Anesthesiology, Perioperative and Pain Medicine, Brigham and Women's Hospital, Harvard Medical School, 20 Shattuck Street, Boston, MA 02115, U.S.A.

Passive SR (sarcoplasmic reticulum) Ca^{2+} leak through the RyR (ryanodine receptor) plays a critical role in the mechanisms that regulate $[Ca^{2+}]_{rest}$ (intracellular resting myoplasmic free Ca^{2+} concentration) in muscle. This process appears to be isoform-specific as expression of either RyR1 or RyR3 confers on myotubes different $[Ca^{2+}]_{rest}$. Using chimaeric RyR3–RyR1 receptors expressed in dyspedic myotubes, we show that isoform-dependent regulation of $[Ca^{2+}]_{rest}$ is primarily defined by a small region of the receptor encompassing amino acids 3770–4007 of RyR1 (amino acids 3620–3859 of RyR3) named as the CLR (Ca^{2+} leak regulatory) region. $[Ca^{2+}]_{rest}$ regulation by the CLR region was associated with alteration of RyRs' Ca^{2+}-activation profile and changes in SR Ca^{2+}-leak rates. Biochemical analysis using Tb^{3+}-binding assays and intrinsic tryptophan fluorescence spectroscopy of purified CLR domains revealed that this determinant of RyRs holds a novel Ca^{2+}-binding domain with conformational properties that are distinctive to each isoform. Our data suggest that the CLR region provides channels with unique functional properties that modulate the rate of passive SR Ca^{2+} leak and confer on RyR1 and RyR3 distinctive $[Ca^{2+}]_{rest}$ regulatory properties. The identification of a new Ca^{2+}-binding domain of RyRs with a key modulatory role in $[Ca^{2+}]_{rest}$ regulation provides new insights into Ca^{2+}-mediated regulation of RyRs.

Key words: calcium-binding site, calcium leak, myotube, skeletal muscle, terbium fluorescence, tryptophan fluorescence.

INTRODUCTION

$[Ca^{2+}]_{rest}$ (intracellular resting myoplasmic free Ca^{2+} concentration) is delicately regulated by the concerted action of multiple Ca^{2+} pathways that co-ordinate Ca^{2+} fluxes from both sarcolemmal membrane and intracellular Ca^{2+} stores [1–3]. In skeletal muscle, Ca^{2+} release from intracellular Ca^{2+} stores is primarily regulated by RyR1 (type 1 ryanodine receptor), which is under the modulation of multiple endogenous protein regulators [4–6]. A role for RyRs on regulating $[Ca^{2+}]_{rest}$ in skeletal muscle was first supported by our studies in dyspedic 1B5 myotubes showing that expression of either RyR1 or RyR3 resulted in significant increase in myoplasmic $[Ca^{2+}]_{rest}$ [7]. More recently, Eltit et al. [3] have confirmed these findings, showing that expression of RyR1 in dyspedic primary myotubes accounted for more than half of the total $[Ca^{2+}]_{rest}$ measured in wild-type cells. Furthermore, the elevation of $[Ca^{2+}]_{rest}$ by expression of RyR1 appears to be the combined effect of both a passive Ca^{2+} leak from a ryanodine-insensitive pool of RyR1 channels (leak channels) and an enhanced basal sarcolemmal Ca^{2+} influx driven by the SR (sarcoplasmic reticulum) Ca^{2+} leak [3,8].

Studies in dysgenic myotubes that lack expression of the DHPR (dihydropyridine receptor) α_{1S} subunit suggest further that negative regulation of RyR1 function by the DHPR also contributes to modulating the passive Ca^{2+} leak responsible for $[Ca^{2+}]_{rest}$ [2,9]. In apparent agreement with these findings, the expression of RyR3, which does not interact with DHPR and is therefore not subject to its negative regulation, results in dyspedic myotubes with $[Ca^{2+}]_{rest}$ that are significantly higher than those restored by the expression of RyR1 [7]. However, expression of RyR2 in dyspedic myotubes confers $[Ca^{2+}]_{rest}$ similar to that of RyR1 [10] despite the fact that, like RyR3, RyR2 also lacks negative regulation by DHPR. These results led us to hypothesize that, in addition to ryanodine-insensitive RyRs and negative regulation by DHPR, other channel properties, which are likely to be unique to each isoform of RyR, also contribute to modulating the passive SR Ca^{2+} leak responsible for $[Ca^{2+}]_{rest}$ regulation.

To test this hypothesis, we took advantage of the remarkable differences in channel function and $[Ca^{2+}]_{rest}$ modulation conferred by RyR1 and RyR3 [7,11–13] to identify the specific molecular determinants within the primary sequence of RyR1 and RyR3 that define the distinctive $[Ca^{2+}]_{rest}$ regulatory properties of each isoform. Using a library of chimaeric RyR3–RyR1 and RyR1–RyR3 receptors expressed in dyspedic myotubes, we show that the ability of the RyR1 and RyR3 to confer isoform-specific $[Ca^{2+}]_{rest}$ regulation can be traced to a small domain encompassing amino acids 3770–4007 of the C-terminal region of RyR1 (amino acids 3620–3859 of RyR3), which we referred to as the CLR (Ca^{2+} leak regulatory) region. Functional and structural analyses revealed the CLR domain contains a *bona fide* Ca^{2+}-binding domain that modulates the Ca^{2+}-sensing properties of RyRs. These data suggest that modulation of $[Ca^{2+}]_{rest}$ by RyRs is under the direct control of a novel cation-binding region found within the RyRs with molecular properties unique to each isoform.

Abbreviations: $[Ca^{2+}]_{rest}$, intracellular resting myoplasmic free Ca^{2+} concentration; CLR, Ca^{2+} leak regulatory; DHPR, dihydropyridine receptor; fura 2/AM, fura 2 acetoxymethyl ester; HEK, human embryonic kidney; MHS, malignant hyperthermia syndrome; RyR, ryanodine receptor; SERCA1, sarcoplasmic/endoplasmic reticulum Ca^{2+}-ATPase 1; SR, sarcoplasmic reticulum.

[1] These authors contributed equally to this work.

[2] Correspondence may be addressed to either of these authors (email jenny@gsu.edu or cperez@zeus.bwh.harvard.edu).

MATERIALS AND METHODS

Chimaeric RyR3–RyR1 constructs

Chimaeric RyR3–RyR1 and RyR1–RyR3 constructs were designed and cloned as described previously [14–16]. All clones used in the present study have been tested previously and confirmed to express and respond to stimulation by RyR agonists 4-chloro-*m*-cresol and/or caffeine [14–16], thus suggesting that they express functional channels.

Cell culture, infection and Ca^{2+} imaging

Primary dyspedic myotubes were differentiated in a 96-well plate format as reported previously [15,16]. Myotubes were infected with 2.5×10^4 HSV-1 (herpes simplex virus 1) virion particles containing wild-type RyR1, wild-type RyR3 or the chimaeric cDNAs constructs [17]. Cells were loaded with 5 μM fura 2/AM (fura 2 acetoxymethyl ester) and imaged at 510 nm with an intensified 10-bit digital CCD (charge-coupled device) camera (XR-Mega-10, Stanford Photonics) using a DG4 multi-wavelength light source as described previously [18]. SR Ca^{2+} content of cultured myotubes was estimated from both peak amplitude and the area under the curve of the Ca^{2+} transient induced by 40 mM caffeine stimulation in the presence of 1 μM thapsigargin. Fluorescent signal was captured from regions of interest within each myotube at 10 frames/s using Piper-control acquisition software (Stanford Photonics) and expressed as the ratio of signal collected at alternating 340 nm/380 nm excitation wavelength. Ca^{2+}-entry rates were estimated from the rate of dye quench by Mn^{2+} entry in myotubes loaded with 5 μM fura 2/AM as described previously [3,18].

[^{3}H]Ryanodine binding assay

[^{3}H]Ryanodine binding to crude membrane extracts (0.1 mg/ml) was performed at equilibrium (90 min at 37 °C) in the presence of 250 mM KCl, 20 mM Hepes (pH 7.4) and 5 nM [^{3}H]ryanodine (PerkinElmer Life Sciences) in the presence of a cocktail of protease inhibitors (Complete™, EDTA-free, Roche). Free Ca^{2+} concentrations were obtained by combination of 1 mM EGTA with specific amounts of $CaCl_2$ according to calculation with the WEBMAXC Extended program (http://www.stanford.edu/~cpatton/maxc.html). Non-specific binding was determined by incubating the vesicles with 5 μM unlabelled ryanodine. Separation of bound and free ligand was performed by rapid filtration through Whatman GF/B glass fibre filters using a 24-well Brandel cell harvester as described previously [13].

Resting free Ca^{2+} measurements

$[Ca^{2+}]_{rest}$ were obtained by direct measurements on myotubes differentiated in 35-mm-diameter culture dishes using double-barrelled Ca^{2+}-selective microelectrodes as described previously [7,18].

Protein expression and purification

cDNA cassettes encoding either amino acids 3770–4007 of RyR1 (CLR-1) or amino acids 3620–3859 of RyR3 (CLR-3) were cloned into the pCold-II expression vector (Takara™) in-frame downstream of a molecular tag containing a streptavidin-binding peptide and a His_6 tag. An unrelated protein domain encompassing amino acids 1–233 of RyR1 [R1-(1–233)] containing the same tag was also expressed and used as control protein. Clones were expressed in *Escherichia coli* BL21 strain in combination with pG-KJE8 vector (Takara™) encoding five molecular chaperones to optimize protein folding. Protein expression was induced by incubation with 0.2 mM IPTG for 6–8 h at 16 °C in the presence of 1 mg/ml arabinose and 2 ng/ml tetracycline. Cells were then disrupted by sonication in solubilization buffer (20 mM Tris/HCl, pH 7.4, 100 mM KCl, 2 mM EDTA and 0.5 % Triton X-100, supplemented with proteinase inhibitors) and soluble proteins were then purified using Strep-trap affinity columns (GE Healthcare) after centrifugation at 100 000 ***g*** for 90 min. Proteins were eluted with 3 mM desthiobiotin in 10 mM Tris/HCl (pH 7.4) and then washed/concentrated with 10 mM Tris/HCl (pH 7.4) using filtration units with a 10 kDa molecular-mass cut-off. The purity of the isolated protein domains was evaluated using SDS/PAGE as described previously [4].

Intrinsic fluorescence spectroscopy and Tb^{3+} fluorescence

Intrinsic fluorescence spectra were recorded at room temperature (24 °C) using a QM1 fluorescence spectrophotometer (PTI) with a xenon short arc lamp. Tryptophan fluorescence spectra were collected before and after titration with different concentrations of $CaCl_2$ as described previously [19]. Tb^3-binding affinity of CLR-1 and CLR-3 was obtained by Tb^{3+} FRET analysis as described previously [20,21] (see the Supplementary Online Data at http://www.biochemj.org/bj/460/bj4600261add.htm).

Circular dichroism

CD spectra were recorded in the far-UV range (190–260 nm) on a Jasco-810 spectropolarimeter at room temperature using a 0.1-cm-pathlength quartz cuvette. The measurements of purified CLR-1 and CLR-3 regions (12–13 μM) were made in 10 mM Tris/HCl (pH 7.4) with either 1 mM EGTA or 0.5 mM $CaCl_2$. All spectra documented represent the average of at least 15 scans in which the background signal from the buffer has been subtracted from the sample signals. Thermal denaturation curves were obtained from changes in CD signal at 222 nm between 10 °C and 90 °C. Measurements were performed in 10 mM Tris/HCl (pH 7.4) with protein concentrations of 10–15 μM. Thermal transition points were calculated by curve fitting as described previously [20].

RESULTS

$[Ca^{2+}]_{rest}$ level of RyR3–RyR1- and RyR1–RyR3-expressing myotubes

To assess whether the differences in myoplasmic $[Ca^{2+}]_{rest}$ conferred by RyR1 and RyR3 were associated to specific structural/functional domains of each isoform, we measured $[Ca^{2+}]_{rest}$ of dyspedic myotubes expressing a series of chimaeric RyR3–RyR1 constructs spanning the entire primary sequence of RyR1 and RyR3 (Figure 1A). All myotubes presenting $[Ca^{2+}]_{rest}$ greater than that of dyspedic myotubes (>50 nM) were considered to be infected and therefore to express the receptor tested [3]. Western blot analysis of infected myotubes indicates that all chimaeric channels tested were expressed at approximately equal levels and showed no differences in expression of the Ca^{2+}-handling proteins SERCA1 (sarcoplasmic/endoplasmic reticulum Ca^{2+}-ATPase 1) and calsequestrin-1 (Supplementary Figure S1 at http://www.biochemj.org/bj/460/bj4600261add.htm).

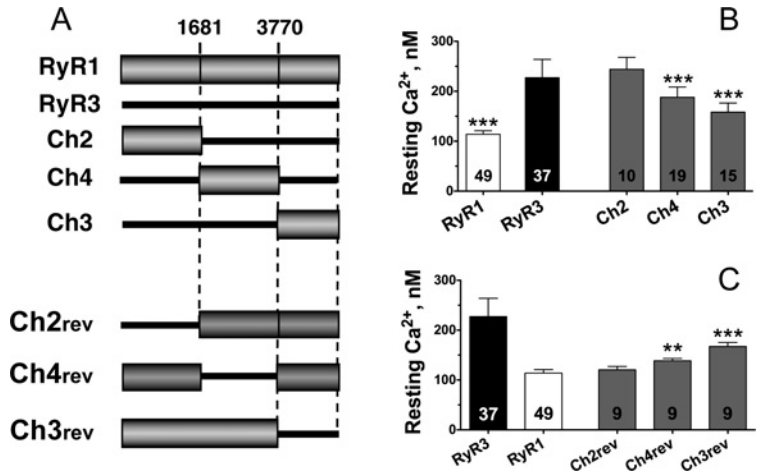

Figure 1 Identification of domains of RyRs important for $[Ca^{2+}]_{rest}$ regulation in cultured myotubes

(**A**) Schematic representation of RyR3-based and RyR1-based chimaeric receptors expressed in dyspedic myotubes. Numbers indicate amino acid positions in RyR1. (**B**) Average $[Ca^{2+}]_{rest}$ values restored by expression of wild-type RyR1, wild-type RyR3 and chimaeric channels Ch2, Ch4 and Ch3. $^{***}P < 0.001$ compared with wild-type RyR3. (**C**) Average $[Ca^{2+}]_{rest}$ values of dyspedic myotubes expressing chimaeras Ch2rev, Ch4rev and Ch3rev representing the exact reverse versions of Ch2, Ch4 and Ch3 respectively. Results are means $\pm$ S.D. ($n = 2$–4). $^{**}P < 0.01$ and $^{***}P < 0.001$ in comparison with RyR1. Values inside the bars indicate total cells analysed that presented $[Ca^{2+}]$ greater than dyspedic myotubes (>50 nM).

Figure 1(B) shows that, whereas the average $[Ca^{2+}]_{rest}$ of RyR1-expressing myotubes is approximately 110 nM, RyR3-expressing myotubes had significantly higher average resting free Ca^{2+} levels. Chimaeric constructs Ch4 and Ch3, containing the central and C-terminal region of RyR1 respectively, displayed a significant reduction in $[Ca^{2+}]_{rest}$ when compared with wild-type RyR3. Average $[Ca^{2+}]_{rest}$ conferred by Ch3-expressing cells was 158 ± 18 nM ($n = 15$), a concentration significantly lower than that conferred by chimaera Ch4 [188 ± 20 nM ($n = 19$; $P < 0.001$)], but slightly higher than that observed in wild-type RyR1-expressing cells [114 ± 7 nM ($n = 49$; $P < 0.001$)]. Consistent with these observations, we found that the reverse chimaeric constructs, in which the corresponding Ch4 and Ch3 regions of RyR3 were expressed in a RyR1 background (Ch4rev and Ch3rev), resulted in a significant increase in $[Ca^{2+}]_{rest}$ when expressed in dyspedic myotubes (Figures 1A and 1C). Similar to Ch3, the Ch3rev construct had a more dramatic effect on Ca^{2+} homoeostasis and induced higher $[Ca^{2+}]_{rest}$ than the Ch4rev region (168 ± 8 nM compared with 138 ± 5 nM for Ch3rev and Ch4rev respectively); however, the $[Ca^{2+}]_{rest}$ reached by Ch3rev was lower than that observed in wild-type RyR3-expressing cells ($P < 0.05$).

The critical structural determinant of chimaera Ch4 was mapped further to the smaller overlapping region between chimaeras Ch17 and Ch21 (Figures 2A and 2B), a domain of RyR1 previously found to play a key role in the cross-talk between RyR1 and DHPR [15,16,22]. Subdivision of chimaera Ch3 into three smaller chimaeric constructs showed that the determinant of RyR1 responsible for reduced $[Ca^{2+}]_{rest}$ regulation was confined to a smaller domain of the C-terminal region, within amino acids 3770–4180 of RyR1 (chimaera Ch22, Figures 2A and 2C). To demonstrate that the reduction in $[Ca^{2+}]_{rest}$ regulation by Ch22 was not due to a conformational change, we also tested the reverse chimaera Ch22rev, in which the region Ch22 of RyR3 was expressed into the corresponding region of RyR1 (Figure 3A). Figure 3(B) shows that, as expected, expression of Ch22rev in dyspedic myotubes resulted in $[Ca^{2+}]_{rest}$ that were significantly higher than those observed for wild-type RyR1-expressing myotubes and much closer to those restored by wild-type RyR3 [182 ± 8 nM ($n = 10$) for Ch22rev compared with 114 ± 7 nM ($n = 49$) for RyR1 ($P < 0.001$)]. The average $[Ca^{2+}]_{rest}$ restored by Ch22rev, however, was still lower than those restored by wild-type RyR3 ($P < 0.01$).

Further analysis narrowed down the location of the $[Ca^{2+}]_{rest}$ regulatory domain of region Ch22 of RyR1 to its N-terminal half (Ch25 in Figures 3A and 3C). Dyspedic myotubes expressing Ch25 showed an average $[Ca^{2+}]_{rest}$ value of 133 ± 18 nM ($n = 18$) that was significantly lower than that observed with the larger Ch22 region [162 ± 14 nM ($n = 27$; $P < 0.01$)]. $[Ca^{2+}]_{rest}$ displayed by Ch25-expressing cells was not statistically different from those observed in wild-type RyR1-expressing myotubes ($P > 0.05$; Figure 3B). Overall, these data show that region Ch25, encompassing amino acids 3770–4007 of RyR1 (amino acids 3620–3859 of RyR3, Figure 3C), holds a structural determinant of RyR sequence that confers the Ca^{2+} channel with resting Ca^{2+}-regulatory properties, which are specific to each isoform. Because of the role of this domain in modulating the rate of Ca^{2+} leak through the channel (see below), for simplicity we refer to this domain of RyRs as the CLR region.

Effect of the CLR region on RyRs Ca^{2+} channel function

Several groups have reported significant differences in Ca^{2+} channel properties between RyR1 and RyR3 [11–13,23]. To assess whether the effect of the CLR region of RyRs on $[Ca^{2+}]_{rest}$ regulation of dyspedic myotubes was associated to alterations in channel properties, we further analysed the Ca^{2+}-dependence of the chimaeric construct Ch25 using [^{3}H]ryanodine-binding studies. Figure 4(A) shows the average Ca^{2+}-dependence of [^{3}H]ryanodine binding to membrane fractions from HEK (human embryonic kidney)-293 cells expressing either wild-type channels or chimaeric construct Ch25. As reported previously, Ca^{2+}-dependence profiles of wild-type RyR1 and wild-type RyR3 indicate monophasic activation for wild-type RyR1 [$EC_{50} = 0.41 \pm 0.18$ μM ($n = 6$)] and a biphasic activation profile for wild-type RyR3 [$EC_{50(1)} = 0.39 \pm 0.04$ μM and $EC_{50(2)} = 35.1 \pm 18$ μM ($n = 6$)] with a plateau between 1 and 10 μM. Consistent with its predominant RyR3 background, the Ca^{2+}-activation curve of chimaera Ch25 showed a biphasic activation profile, but with a more exacerbated biphasic

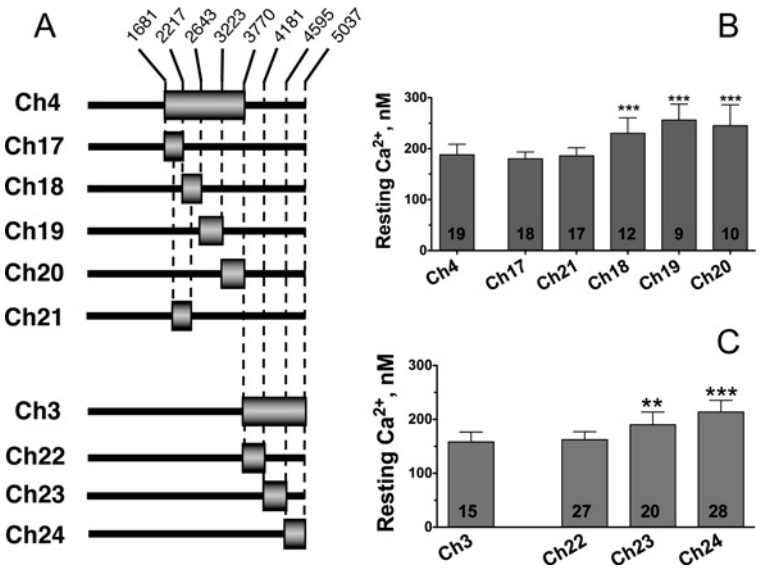

Figure 2 Further localization of the RyR regions responsible for $[Ca^{2+}]_{rest}$ regulation

(**A**) Schematic representation of chimaeric RyR3–RyR1 receptors containing several contiguous subdomains of region Ch4 and Ch3 of RyR1 into the RyR3 background. Numbers indicate amino acid positions in RyR1. (**B** and **C**) Average $[Ca^{2+}]_{rest}$ of myotubes expressing the chimaeric constructs depicted in (**A**). $***P < 0.001$ compared with Ch4 (**B**). $**P < 0.01$ and $***P < 0.001$ in comparison with Ch3 (**C**). Values inside the bars indicate total cells analysed. Results are means $\pm$ S.D. ($n = 2$–5).

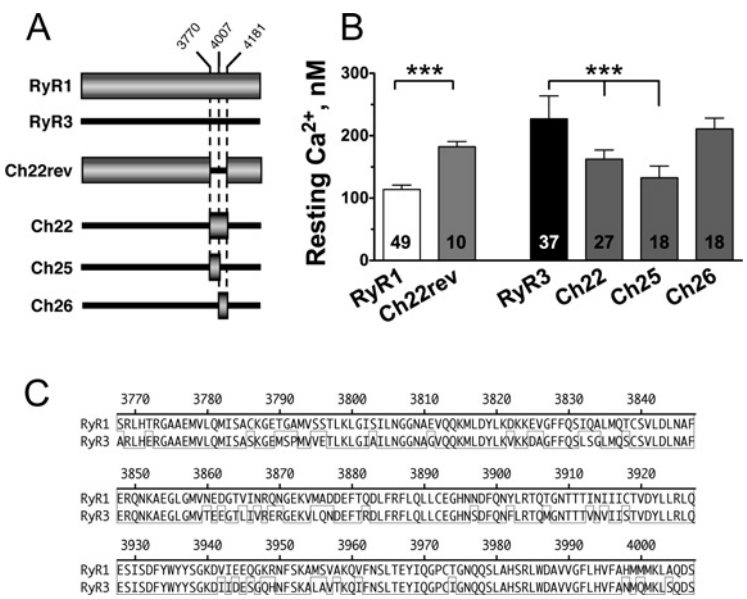

Figure 3 Region Ch22 of RyR3 enhances $[Ca^{2+}]_{rest}$ regulation by RyR1

(**A**) Diagram of reverse chimaera Ch22rev-expressing region Ch22 of RyR3 in a RyR1 background. Additional RyR3-based chimaeras further mapping the CLR region of RyR1 are indicated. (**B**) Average $[Ca^{2+}]_{rest}$ values of dyspedic myotubes expressing constructs depicted in (**A**). Results are means $\pm$ S.D. ($n = 2$–4). Note that region Ch22 of RyR3 confers on chimaera Ch22rev significantly higher $[Ca^{2+}]_{rest}$ regulatory properties than that of the wild-type RyR1 channel, which is similar to that of wild-type RyR3. Further subdivision of region Ch22 into smaller domains Ch25 and Ch26 localized the $[Ca^{2+}]_{rest}$ regulatory region at amino acids 3770–4007 of RyR1 and amino acids 3620–3859 of RyR3 (Ch25). (**C**) Amino acid alignment of the CLR region from RyR1 and RyR3 using the Clustal method. Boxed sequence indicate identical residues, and the rule indicates the amino acid position in RyR1.

Ca^{2+} response and a wider activation plateau (1–100 μM; Figure 4) than wild-type RyR3 [$EC_{50(1)} = 0.36 \pm 0.03$ μM and $EC_{50(2)} = 465.7 \pm 120$ μM ($n = 4$)]. [^{3}H]Ryanodine-binding analysis of Ca^{2+} inhibition revealed that Ca^{2+}-sensitivity for inactivation of RyR3 was 6–7-fold lower than that of RyR1 ($IC_{50} = 0.44 \pm 0.22$ mM for RyR1 compared with $IC_{50} = 2.68 \pm 0.77$ mM for RyR3). Analysis of Ca^{2+} inactivation for chimaera Ch25 showed a significantly reduced sensitivity to Ca^{2+} inhibition compared with wild-type RyR1, but similar to that of wild-type RyR3 ($IC_{50} = 3.01 \pm 0.97$ mM, Figure 4B). Comparison of the [^{3}H]ryanodine-binding data expressed as a fraction of the basal activity (B/B_{min}) shows important differences in channel function between wild-type RyR1 and wild-type RyR3, with RyR3 reaching noticeably higher activation levels than RyR1 (Figure 4C). Like RyR3, chimaera Ch25 also displays high activation levels, suggesting that, despite changes in its

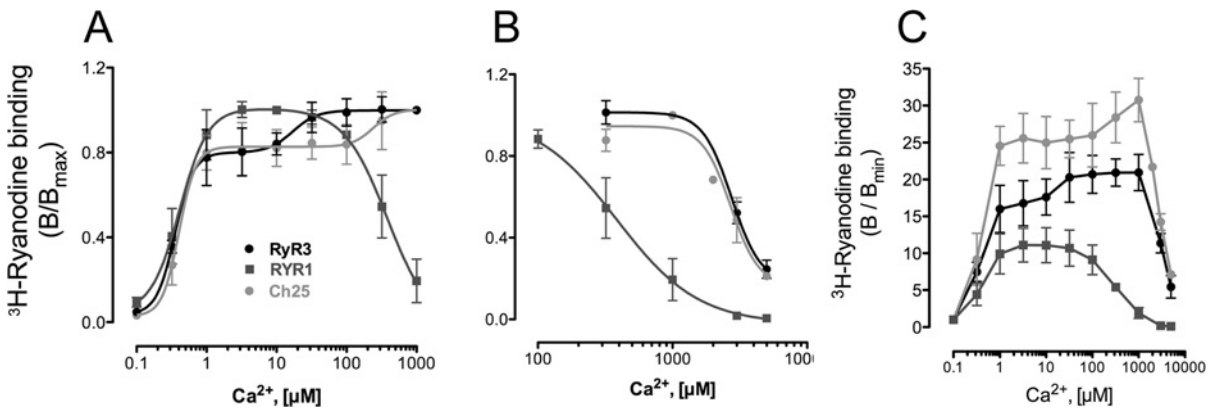

Figure 4 CLR region modulates the Ca^{2+}-dependence function of RyRs

RyR channel function was assessed by specific [^{3}H]ryanodine binding to crude membrane preparation from HEK-293 cells permanently transformed with wild-type RyR1, wild-type RyR3 or chimaera Ch25. (**A**) Normalized Ca^{2+}-activation curve for RyR1 (squares), RyR3 (dark circles) and Ch25 (grey circles). RyR1 is fitted to a monophasic Hill equation, whereas RyR3 and Ch25 are fitted to the biphasic Hill equations. (**B**) Normalized Ca^{2+}-inhibition curves for wild-type RyR1, wild-type RyR3 and Ch25 fitted to a monophasic equation. (**C**) Ca^{2+}-dependence of [^{3}H]ryanodine binding expressed as the fraction of B_{min} showing that channel activity of chimaera Ch25 preserves the same functional profile of RyR3. Activation and inhibition profiles are the combined result of four to six experiments performed in duplicate or triplicate from multiple HEK-293 membrane preparations. Results are means ± S.E.M. ($n = 4$–6).

Table 1 Curve fit statistics for [^{3}H]ryanodine-binding analyses of Ca^{2+} activation

Results are means ± S.D. *$P < 0.001$ (one-way ANOVA with Tukey's post-hoc analysis).

Construct	$EC_{50(1)}$ (μM)	$EC_{50(2)}$ (μM)	n
RyR1	0.41 ± 0.18	N/A	6
RyR3	0.39 ± 0.04	35.1 ± 18*	6
Ch25	0.36 ± 0.03	465.7 ± 120*	4

Table 2 Curve fit statistics for [^{3}H]ryanodine-binding analyses of Ca^{2+} inhibition

Results are means ± S.D.

Construct	IC_{50} (mM)	n
RyR1	0.44 ± 0.22	4
RyR3	2.68 ± 0.77	4
Ch25	3.01 ± 0.97	5

Ca^{2+}-activating profile, chimaera Ch25 preserves most of the channel function characteristic of RyR3. The curve fit and statistics of Ca^{2+} activation and inhibition for wild-type and chimaeric receptors are presented in Tables 1 and 2. Overall, these data suggest that substitution of the CLR region of RyRs results in significant changes in the Ca^{2+} activation properties of the chimaeric channels.

Effect of the CLR region on myoplasmic Ca^{2+} fluxes

Because of the importance of Ca^{2+} flux equilibrium to myoplasmic $[Ca^{2+}]_{rest}$ regulation, we also assessed whether CLR-mediated changes in the Ca^{2+}-sensing properties of RyRs had an effect on the rate of SR Ca^{2+} leak or rate of sarcolemmal Ca^{2+} entry in dyspedic myotubes expressing either wild-type or Ch25 constructs. SR Ca^{2+} leak was estimated using the differences in SR Ca^{2+} load measured by the magnitude of Ca^{2+} release induced by a 40 mM caffeine challenge in the presence of the SERCA1 pump inhibitor thapsigargin. Figure 5(A) shows that myotubes expressing wild-type RyR1 generated caffeine-induced Ca^{2+} release transients that were significantly larger than those of myotubes expressing wild-type RyR3. Analysis of average Ca^{2+} transient revealed no significant differences in peak transient amplitude between isoforms (Figure 5B). However, the total Ca^{2+} released in RyR3-expressing myotubes, which was measured as the integral of the fluorescent signal, was found to be significantly reduced (Figure 5C), indicating an enhanced SR Ca^{2+} leak. Consistent with this smaller SR Ca^{2+} load, RyR3-expressing myotubes also displayed significantly higher rates of Mn^{2+} quench than RyR1-expressing myotubes (Figures 5D and 5E) revealing increased rates of sarcolemmal Ca^{2+} entry at rest. By comparison, Ch25-expressing cells displayed SR Ca^{2+} release at levels between RyR1 and RyR3, showing similar peak Ca^{2+} transient amplitude, but with significantly increased total Ca^{2+} release compared with wild-type RyR3-expressing cells (Figures 5A–5C). Likewise, Ch25-expressing myotubes showed rates of resting Mn^{2+} quench similar to those of RyR1-expressing cells and significantly lower than those of RyR3-expressing myotubes (Figures 5D and 5E). These data suggest that myotubes expressing Ch25 and RyR1 present similar rates of SR Ca^{2+} leak and that the differences in SR Ca^{2+} load observed between Ch25 and RyR1 (Figure 5C) are likely to be the result of reduced sensitivity to Ca^{2+} inhibition displayed by Ch25 (Figure 4) that allows for a faster emptying of the Ca^{2+} stores than RyR1. These findings are consistent with previous studies indicating increased basal channel function of RyR3 [24–27] and suggest that the insertion of the CLR region of RyR1 into the RyR3 sequence (chimaera Ch25) results in less leaky channels.

Expression and purification of the CLR region

[^{3}H]Ryanodine-binding studies suggest the CLR region may be involved in Ca^{2+}-mediated activation of RyRs. To evaluate a direct role of this region in modulating the Ca^{2+}-sensing properties of RyRs, a fragment comprising the CLR region of RyR1 (amino acids 3770–4007, herein CLR-1) and the corresponding fragment

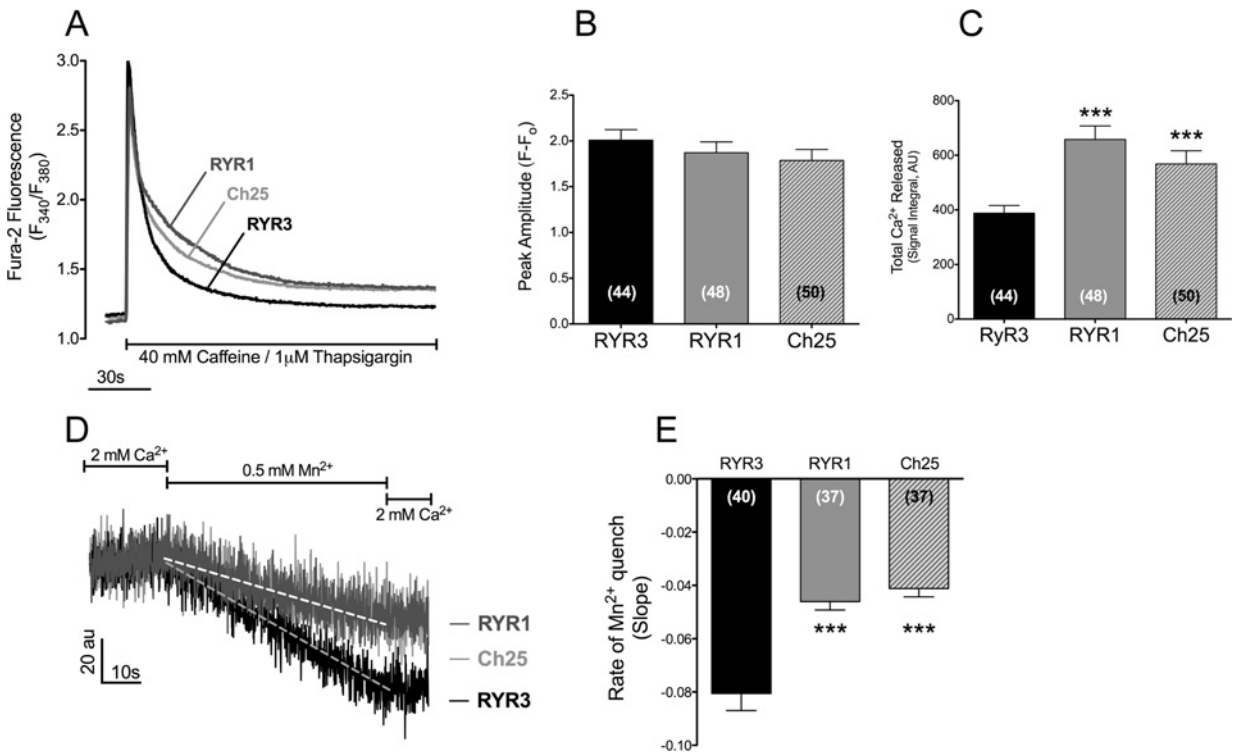

Figure 5 Exchange of CLR regions among isoforms of RyR modulate SR Ca^{2+} leak and sarcolemmal Ca^{2+} entry

(**A**) Average caffeine-induced Ca^{2+}-release transients of fura 2-loaded dyspedic myotubes expressing wild-type RyR1, wild-type RyR3 or chimaera Ch25. S.D. of the traces has been omitted for clarity. Average peak Ca^{2+} transient amplitude (**B**) and total Ca^{2+} release (**C**) are shown for each population of myotubes. ***$P < 0.001$ in comparison with wild-type RyR3. (**D**) Representative traces of Mn^{2+} quench of fura 2 fluorescence of RyR1- and RyR3-expressing myotubes showing differences in resting sarcolemmal Ca^{2+} entry among isoforms. (**E**) Average rate of Mn^{2+} quench, calculated from the slope of the fluorescent signal (broken lines), is shown for each set of constructs. Results are means $\pm$ S.E.M. for a total of nine or ten individual cultured wells ($n = 3$). Values in parentheses indicate total myotubes analysed.

in RyR3 (amino acids 3620–3859, herein CLR-3), were expressed in *E. coli* BL21 cells and analysed for their ability to bind Ca^{2+}. In order to minimize misfolding of the protein domains, the CLR fragments were expressed in the presence of five chaperone proteins, to assist in protein folding, and then purified from the soluble fraction of the cell homogenate to avoid using inclusion bodies. All purified domains, including control region R1-(1–233), showed approximately 95 % purity and molecular masses of approximately 30 kDa, consistent with their predicted 25–27 kDa molecular mass (Figure 6A).

Conformational analysis of CLR domains

Far-UV CD analysis of CLR-1 and CLR-3 indicate that both purified protein domains exhibit helical conformation (Figures 6C and 6D). The well-folded secondary structure of these fragments is consistent with the fact that intrinsic tryptophan fluorescence emission of the CLR regions peak at 330 nm (see Figure 8), and suggests that the tryptophan residues are largely buried within this folded conformation [28]. Moreover, analysis of thermal transition revealed important differences in thermal stability between CLR-1 and CLR-3 (Figure 6B). CLR-1 appeared to be more stable than CLR-3 with approximately 10 °C difference in melting temperature ($T_m = 61.5 \pm 0.2$ °C and 51.7 ± 0.3 °C for CLR-1 and CLR-3 respectively) and a more co-operative thermal unfolding curve than RyR3. These data are consistent with isoform-specific differences in domain packing and suggest that the CLR region of RyR3 displays a higher degree of molecular flexibility than its RyR1 counterpart.

Metal-binding properties of the CLR domain

Upon addition of 0.5 mM Ca^{2+}, both domain fragments displayed a small, but reproducible, decrease in mean residue ellipticity (205–225 nm) indicating Ca^{2+} changes in secondary structure (Figures 6C and 6D), therefore Ca^{2+} interaction with the CLR domains. Interestingly, the effects of Ca^{2+} in secondary structure of CLR-1 were significantly more pronounced than the changes observed in CLR-3. Direct cation binding was assessed using Tb^{3+} fluorescence analysis. This binding assay is commonly used to determine Ca^{2+}-binding sites because Tb^{3+} has a similar ionic radius and metal–co-ordination chemistry to that of Ca^{2+}, while allowing for quantitative analysis [29,30]. As shown in Figure 7, titration of the purified CLR-1 and CLR-3 domains with micromolar concentrations of $TbCl_3$ resulted in a significant increase in fluorescent signal at 545 nm when excited at 280 nm. Both CLR domains showed monophasic binding curves with CLR-1 displaying significantly higher binding affinity for Tb^{3+} than domain CLR-3 [$K_d = 0.86 \pm 0.07$ μM for CLR-1 compared with 3.8 ± 0.5 μM for CLR-3 ($n = 3$; $P < 0.001$); Figures 7B and 7D and Table 2], supporting further the existence of a cation-binding pocket with moderate affinity within the primary structure of the CLR region of RyR1 and RyR3.

To characterize further the Ca^{2+}-binding properties of the cation-binding pocket, we next analysed Ca^{2+}-induced

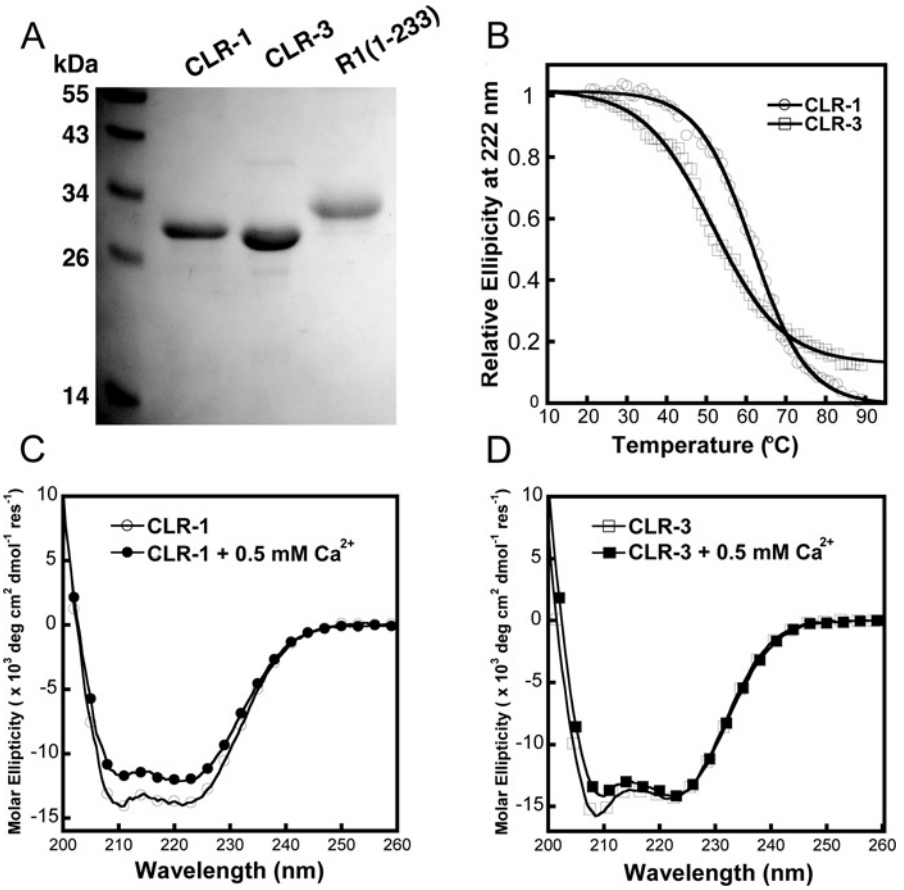

Figure 6 Purification and conformational analysis of the CLR region of RyR1 and RyR3

(**A**) Coomassie Blue-stained SDS/PAGE gel loaded with 2 μg/lane CLR-1, 4 μg/lane CLR-3 and 3 μg/lane R1-(1–233) purified from *E. coli* BL21 cells. (**B**) Representative thermal stability curves for CLR-1 and CLR-3 showing changes in CD signal at 222 nm ($n = 2$). (**C** and **D**) Comparison of far-UV CD spectra of purified CLR-1 (circles) and CLR-3 (squares) regions in the presence of 1 mM EGTA (unfilled symbols) indicating high α-helix content and small differences in secondary/tertiary structure between isoforms. Note the small but reproducible decrease in ellipticity of the CD spectra in the presence of 0.5 mM Ca^{2+} (filled symbols).

conformational changes in the purified domains by monitoring intrinsic tryptophan fluorescence. As shown in Figures 8(A) and 8(C), upon titrating with increasing concentrations of Ca^{2+} both domain fragments displayed a large decrease in tryptophan fluorescence. By comparison, Ca^{2+} titration of a control unrelated fragment of RyR1 [R1-(1–233)], containing amino acids 1–233 of RyR1, showed only marginal fluorescence changes upon Ca^{2+} addition (Figures 8B and 8D). This region of RyR1 has been crystallized previously and its atomic structure has confirmed the absence of formal cation-binding sites [31]. These fluorescence data are consistent with the Ca^{2+}-induced conformational changes revealed by the CD spectroscopy assay and suggest that Ca^{2+} binding detected by the tryptophan fluorescence is specific to the CLR domains.

Unlike the Tb^{3+} titration assay, Ca^{2+} titration of tryptophan fluorescence was better fitted to a biphasic Ca^{2+}-binding process (Figures 8B and 8D). This biphasic profile was particularly evident in CLR-3 with Ca^{2+}-binding affinities in the micromolar range ($K_{d1} = 7.3 \pm 0.3\ \mu M$ and $K_{d2} = 18.4 \pm 1.6\ \mu M$). The biphasic binding profile of domain CLR-1 was less pronounced with K_{d1} of $11.0 \pm 1.8\ \mu M$ and K_{d2} of $21.6 \pm 2.7\ \mu M$. Whereas average K_{d1} showed a slight, but significant, difference between CLR-1 and CLR-3, there was no difference seen in average K_{d2}, suggesting that the CLR region of RyR1 and RyR3 may present slightly different Ca^{2+}-binding properties (Table 3). The high Hill coefficients of the CLR domains are suggestive of several ligand-binding sites; however, other factors such as the ligand-induced change in protein conformation may also contribute to this high level of co-operativity [32].

Table 3 Curve fit statistics for Tb^{3+}- and Ca^{2+}-binding analyses of purified CLR domains

Results are means $\pm$ S.D. $^*P < 0.05$ compared with K_{d2}; $^{***}P < 0.001$ compared with CLR-1 (Student's *t* test).

	Tb^{3+} (μM)	Ca^{2+} (μM)		
Domain	K_d	K_{d1}	K_{d2}	Hill coefficient
CLR-1	0.9 ± 0.1	$11.0 \pm 1.8^*$	21.6 ± 2.7	4.9 ± 0.5
CLR-3	$3.8 \pm 0.5^{***}$	$7.3 \pm 0.3^*$	18.4 ± 1.6	6.7 ± 1.8

DISCUSSION

In a previous study, we showed that expression of RyR1 and RyR3 in cultured dyspedic myotubes has a dramatic effect in the resting Ca^{2+} regulation where RyR3 restored myoplasmic

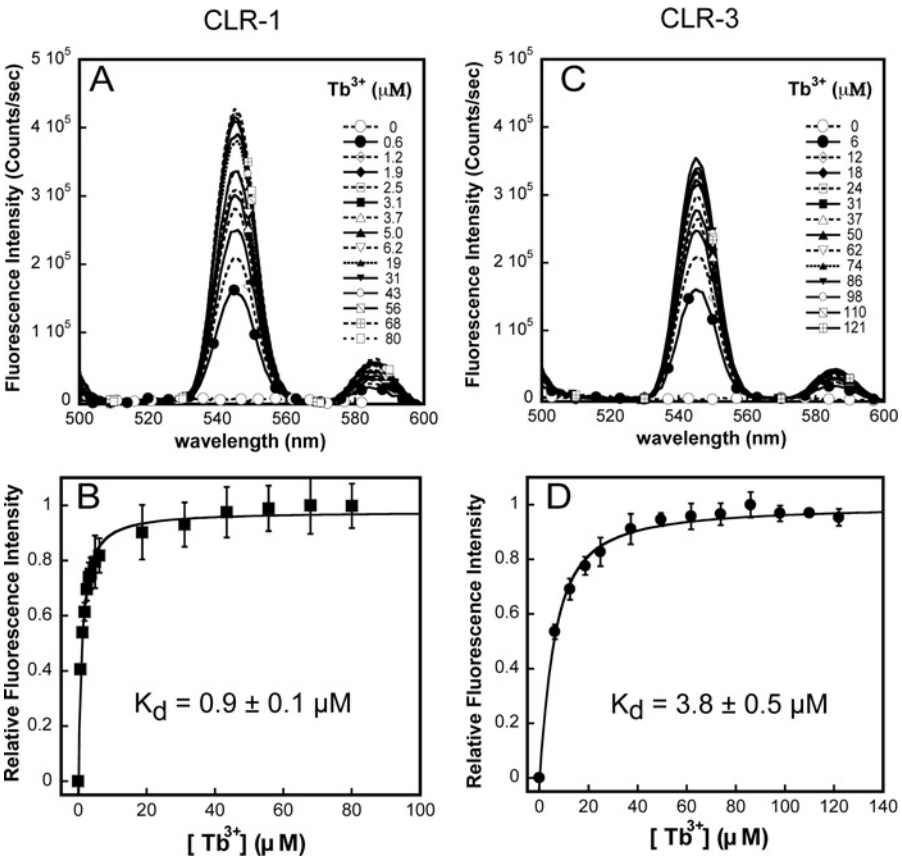

Figure 7 CLR-1 and CLR-3 domains bind Tb^{3+} with high affinity

Representative Tb^{3+} fluorescence spectra of purified CLR-1 (**A**) and CLR-3 (**C**) regions showing an increase in fluorescence intensity at 545 nm upon titration with Tb^{3+} (excitation at 280 nm). Tb^{3+} binding to CLR-1 (**B**) and CLR-3 (**D**) domains is expressed as the average change in relative fluorescence intensity ($[F_i - F_{min}]/[F_{max} - F_{min}]$). Data were fitted to monophasic binding curves using eqn (S3) (see the Supplementary Online Data at http://www.biochemj.org/bj/460/bj4600261add.htm). Results are means ± S.D. ($n = 3$).

$[Ca^{2+}]_{rest}$ to significantly higher Ca^{2+} levels than RyR1 [7]. In the present study, we used a series of chimaeric RyR channels spanning the entire sequence of RyR1 and RyR3 in order to localize and characterize the molecular determinant of each isoform responsible for their differential effect on $[Ca^{2+}]_{rest}$.

Location of the resting Ca^{2+}-regulatory domain of RyRs

We found that the ability of RyR1 and RyR3 to differentially modulate $[Ca^{2+}]_{rest}$ can be traced to two regions of the primary sequence: one is the overlapping region between chimaeras Ch17 and Ch21 (17/21, amino acids 1924–2217 of RyR1 and 1798–2082 of RyR3) and the other the CLR region encompassing amino acids 3770–4007 of RyR1 (amino acids 3620–3859 of RyR3). The impact of region 17/21 on $[Ca^{2+}]_{rest}$ regulation was shown to be less dramatic than that of the CLR region in both the RyR3-based (Ch4) and the RyR1-based (Ch4rev) chimaeric constructs. Our previous studies of these chimaeric receptors have shown that the RyR1 region encompassing region 17/21 is directly involved in the cross-talk between DHPR and RyR1, and confers RyR3 with the ability to restore DHPR tetrad formation, DHPR retrograde signalling and excitation–contraction coupling [15,16,22]. Therefore it is likely that the mild reduction in $[Ca^{2+}]_{rest}$ observed in dyspedic myotubes expressing Ch4, Ch21 or Ch17 could be related to an enhanced orthograde regulation by DHPR that inhibited RyR1 function, thereby restricting overall SR Ca^{2+}-leak, similar to the mechanism described by Eltit et al. [2,3]. Nonetheless, an effect of altered Ca^{2+} regulation by Ch4, Ch21 and Ch17 on the rates of SR Ca^{2+} leak and its subsequent effect on $[Ca^{2+}]_{rest}$ should not be ruled out as all these chimaeric constructs have shown to affect both Ca^{2+}-activation and Ca^{2+}-inhibition profiles of the channel [13].

The CLR regions of RyR1 and RyR3 were shown to have a more dramatic effect on Ca^{2+} homoeostasis conferring on chimaeric receptors $[Ca^{2+}]_{rest}$-regulatory properties distinctive of the specific CLR sequence being expressed, regardless of the overall amino acid background. In contrast with region 17/21, it is unlikely that the effect the CLR region has on $[Ca^{2+}]_{rest}$ could be related to orthograde regulation by DHPR, as cumulative evidence indicates that the C-terminal region of RyR1 is not involved in cross-talk with the DHPR complex. Our previous studies involving several chimaeric RyR3–RyR1 channels, including Ch25 used in the present study, have shown that exchange of various RyR domains containing the CLR region had a negligible effect on either excitation–contraction coupling [14] or DHPR Ca^{2+} current densities [15,16,22], suggesting that the RyR region encompassing the CLR region is not involved directly in the DHPR–RyR interaction.

Importantly, and consistent with our previous studies in wild-type RyR3 and wild-type RyR1 [7], Western blot analysis indicates that all chimaeric constructs displayed similar

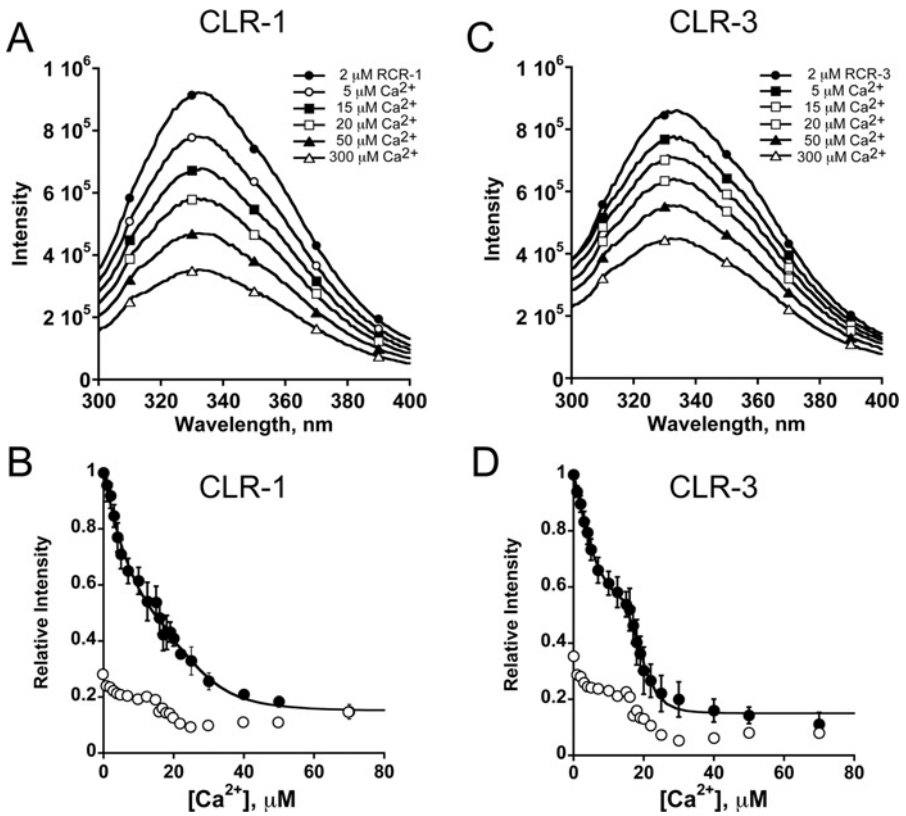

Figure 8 Characterization of the Ca^{2+}-binding properties of CLR-1 and CLR-3

Representative fluorescence emission spectra showing a Ca^{2+}-induced decrease in intrinsic tryptophan fluorescence intensity of CLR-1 (**A**) and CLR-3 (**C**) domains excited at 280 nm (filled circles). Ca^{2+} titration curves were fitted to a biphasic binding process using eqns (S1) and (S2) (see the Supplementary Online Data at http://www.biochemj.org/bj/460/bj4600261add.htm) (**B** and **D**). Results are mean ± S.D. relative fluorescence intensity ($n = 3$). Ca^{2+}-induced changes in relative fluorescence intensity of control protein R1-(1–233) (**B** and **D**, unfilled circles) are shown as fractions of the maximal response of either CLR-1 or CLR-3.

expression levels when transfected in dyspedic myotubes. Therefore changes in $[Ca^{2+}]_{rest}$ like the one caused by exchange of the CLR region could not be explained simply by changes in expression levels of the chimaeric channels.

Chronically elevated $[Ca^{2+}]_{rest}$ is a common feature of skeletal muscle cells expressing RyR1 mutations linked to MHS (malignant hyperthermia syndrome). Extensive functional analysis of muscle cells expressing numerous MHS-linked mutations of RyR1 has revealed that elevated $[Ca^{2+}]_{rest}$ is often associated with alteration of Ca^{2+} and Mg^{2+} regulation of RyR1 [3,8,33–38], with a number of these mutations being confirmed to result in increased basal Ca^{2+} channel function that leads to enhanced passive SR Ca^{2+} leak [8,34,36,39]. The reverse mechanism seems to operate in chimaera Ch25 where the insertion of the more stable CLR region of RyR1 into the RyR3 sequence appeared to attenuate the enhanced basal channel function of RyR3, causing myotubes to decrease both overall SR Ca^{2+} leak and sarcolemmal Ca^{2+} entry, resulting in a subsequent reduction of $[Ca^{2+}]_{rest}$. These results are also in agreement with the cell boundary theorem that predicts permanent changes in cytosolic Ca^{2+} concentration as a result of steady changes of sarcolemmal Ca^{2+} fluxes [1].

Molecular properties of the CLR region

The identification of *bona fide* Ca^{2+}-binding sites in the CLR region of RyR1 and RyR3 with Ca^{2+} affinities within the physiological range seems in agreement with a role for the CLR region in Ca^{2+}-mediated regulation of RyRs. However, whether Ca^{2+} binding to the CLR region is involved directly in Ca^{2+}-mediated activation of RyRs needs further study. Our *in vitro* biochemical characterization (Ca^{2+} titration) of the isolated CLR domains suggests that Ca^{2+}-binding affinities of CLR-1 and CLR-3 are similar. It therefore seems unlikely that the shift of Ca^{2+}-sensing properties resulting from the exchange of CLR region in chimaera Ch25 could be explain by the overall Ca^{2+}-binding properties of the CLR region alone. Instead, our conformational analysis suggests significant differences in overall molecular conformation between the CLR regions of RyR1 and RyR3. Differences in the secondary/tertiary structure between CLR-1 and CLR-3 are supported by CD analysis, which revealed slight differences in helical content among domains (Figures 6C and 6D). This difference in folded conformation is also evident from the differential effect of Ca^{2+} in the CD spectra. Indeed, whereas Ca^{2+} addition resulted in changes in the overall conformation of CLR-1, it had significantly less effect on the folded structure of CLR-3. This is supported further by thermal transition studies (Figure 6B) that revealed important differences in thermal stability and unfolding co-operativity between CLR domains, with the overall structure of CLR-3 being less stable and packed than that of CLR-1.

An intriguing result was the differences in binding profile (monophasic compared with biphasic) and affinity of the cation-binding pocket detected by Tb^{3+}- and Ca^{2+}-binding assays. These differences probably arise from the intrinsic differences in which

each assay reads out cation–protein interaction. Whereas changes in tryptophan fluorescence are the result of global conformational changes of the CLR domain, the Tb^{3+} fluorescence signal is the result of energy transfer between nearby tryptophan residues and Tb^{3+}, and therefore primarily reflects local events that are highly sensitive to molecular distance. A monophasic binding profile like the one observed during Tb^{3+} titration could stem from the fact that tryptophan residues were present in close proximity to only one of the Tb^{3+}-binding sites. This seems consistent with the actual location of the two tryptophan residues of the CLR region, which are found close to each other and clustered towards the C-terminal end of the domain (Figure 3C).

At the functional level, biphasic Ca^{2+}-activating profiles like the one observed in our [^{3}H]ryanodine-binding studies have been reported previously in RyR3 [13] and RyR2 [40,41] and are consistent with our hypothesis that activation of RyRs may involve at least two moderately co-operative Ca^{2+}-activation sites [13]. The binding of Ca^{2+} to multiple sites in a highly co-operative manner have been shown to facilitate protein responses to small changes in Ca^{2+} concentration [42,43]. The high degree of co-operativity to Ca^{2+}-binding showed by the CLR domains (Table 3) and the effects of these domains in the Ca^{2+}-activation profile of chimaeric receptors are consistent with this idea. These data suggest that Ca^{2+}-dependent activation of RyR channels may be a complex event possibly involving multiple Ca^{2+}-binding sites.

It is worth noting that the RyR1 sequence around the CLR has been previously associated with Ca^{2+} regulation with several potential Ca^{2+}-binding and/or Ca^{2+}-regulatory sites being reported in a number of studies (Supplementary Figure S2 at http://www.biochemj.org/bj/460/bj4600261add.htm). Even though the nature of the Ca^{2+}-binding sites at the CLR region is currently unknown, it appears that the amino acid ligands that conform the Ca^{2+}-binding domain(s), do not group as continuous canonical EF-hand motif, but rather as a discontinuous array. This is not surprising as an analysis of the atomic structure of more than 1600 Ca^{2+}-binding domains have shown that discontinuous non-EF-hand binding sites account for more than 90 % of the known structures [44]. To our knowledge, this is the first report linking amino acids 3770–4007 of RyR1 (3620–3859 of RyR3) to either direct Ca^{2+}-binding or $[Ca^{2+}]_{rest}$ regulation. Previous studies have associated this same region with interaction to S100A1 [45], a Ca^{2+}-binding protein known to modulate Ca^{2+} cycling in skeletal muscle through its interaction with the calmodulin-binding site of RyR1 [46,47]. However, it is unlikely that the effects of the CLR region in $[Ca^{2+}]_{rest}$ regulation observed in our study could be linked to binding of S100A1 because S100A1-null muscle fibres appear to present normal $[Ca^{2+}]_{rest}$ regulation [46].

Overall, our data revealed that the region of amino acids 3770–4007 of RyR1 (amino acids 3620–3859 of RyR3) encompasses a novel Ca^{2+}-binding domain that provide RyR with unique conformational properties that define their distinctive modulatory role in $[Ca^{2+}]_{rest}$ regulation. Because this modulatory role appears to be linked directly to the ability of RyRs to regulate passive SR Ca^{2+} leak [2,3], it is conceivable that the effect of the CLR region on $[Ca^{2+}]_{rest}$ could result from changes in RyR susceptibility to adopt the leak conformation. Our data, however, do not rule out the possibility that changes in gating properties of the functional pool of RyRs could also contribute to modulate the overall SR Ca^{2+} content that drives sarcolemmal Ca^{2+} fluxes and thereby $[Ca^{2+}]_{rest}$ regulation. Lastly, the identification of this new Ca^{2+}-binding domain in RyRs, which was found to play a key role in modulating myoplasmic $[Ca^{2+}]_{rest}$, provides new insights into Ca^{2+}-mediated regulation of RyRs function.

AUTHOR CONTRIBUTION

Claudio Perez conceived the study, designed the experiments and wrote the paper. Jose Lopez performed $[Ca^{2+}]_{rest}$ measurements and edited the paper before submission. Yanyi Chen performed conformational analysis, thermal stability and Tb^{3+} FRET studies. Shenghui Xue performed the metal-binding experiments. Juan Zou performed gel analysis of protein variants. Jenny Yang designed the experiments and contributed to preparation of the paper.

ACKNOWLEDGEMENTS

We thank Dr P.D. Allen and Dr J.D. Fessenden for kindly providing several chimaeric cDNA constructs and Dr K. Westerman for her assistance with editing of the paper before submission.

FUNDING

This work was supported by the National Institutes of Health [grant numbers 5K01AR054818 (to C.F.P.), and GM081749 and EB007268 (to J.J.Y.)] and by the William S. Milton Fund/Harvard Medical School (to C.F.P.).

REFERENCES

1 Rios, E. (2010) The cell boundary theorem: a simple law of the control of cytosolic calcium concentration. J. Physiol. Sci. **60**, 81–84 CrossRef PubMed
2 Eltit, J. M., Li, H., Ward, C. W., Molinski, T., Pessah, I. N., Allen, P. D. and Lopez, J. R. (2011) Orthograde dihydropyridine receptor signal regulates ryanodine receptor passive leak. Proc. Natl. Acad. Sci. U.S.A. **108**, 7046–7051 CrossRef PubMed
3 Eltit, J. M., Yang, T., Li, H., Molinski, T. F., Pessah, I. N., Allen, P. D. and Lopez, J. R. (2010) RyR1-mediated Ca^{2+} leak and Ca^{2+} entry determine resting intracellular Ca^{2+} in skeletal myotubes. J. Biol. Chem. **285**, 13781–13787 CrossRef PubMed
4 Boncompagni, S., Thomas, M., Lopez, J. R., Allen, P. D., Yuan, Q., Kranias, E. G., Franzini-Armstrong, C. and Perez, C. F. (2012) Triadin/Junctin double null mouse reveals a differential role for Triadin and Junctin in anchoring CASQ to the jSR and regulating Ca^{2+} homeostasis. PLoS ONE **7**, e39962 CrossRef PubMed
5 Fill, M. and Copello, J. A. (2002) Ryanodine receptor calcium release channels. Physiol. Rev. **82**, 893–922 PubMed
6 Jiang, J., Zhou, Y., Zou, J., Chen, Y., Patel, P., Yang, J. J. and Balog, E. M. (2010) Site-specific modification of calmodulin Ca^{2+} affinity tunes the skeletal muscle ryanodine receptor activation profile. Biochem. J. **432**, 89–99 CrossRef PubMed
7 Perez, C. F., Lopez, J. R. and Allen, P. D. (2005) Expression levels of RyR1 and RyR3 control resting free Ca^{2+} in skeletal muscle. Am. J. Physiol. Cell Physiol. **288**, C640–C649 CrossRef PubMed
8 Yang, T., Esteve, E., Pessah, I. N., Molinski, T. F., Allen, P. D. and Lopez, J. R. (2007) Elevated resting $[Ca^{2+}]_i$ in myotubes expressing malignant hyperthermia RyR1 cDNAs is partially restored by modulation of passive calcium leak from the SR. Am. J. Physiol. Cell Physiol. **292**, C1591–C1598 CrossRef PubMed
9 Esteve, E., Eltit, J. M., Bannister, R. A., Liu, K., Pessah, I. N., Beam, K. G., Allen, P. D. and Lopez, J. R. (2010) A malignant hyperthermia-inducing mutation in RYR1 (R163C): alterations in Ca^{2+} entry, release, and retrograde signaling to the DHPR. J. Gen. Physiol. **135**, 619–628 CrossRef PubMed
10 Lee, E. H., Lopez, J. R., Li, J., Protasi, F., Pessah, I. N., Kim, D. H. and Allen, P. D. (2004) Conformational coupling of DHPR and RyR1 in skeletal myotubes is influenced by long-range allosterism: evidence for a negative regulatory module. Am. J. Physiol. Cell Physiol. **286**, C179–C189 CrossRef PubMed
11 Chen, S. R., Li, X., Ebisawa, K. and Zhang, L. (1997) Functional characterization of the recombinant type 3 Ca^{2+} release channel (ryanodine receptor) expressed in HEK293 cells. J. Biol. Chem. **272**, 24234–24246 CrossRef PubMed
12 Murayama, T. and Ogawa, Y. (2004) RyR1 exhibits lower gain of CICR activity than RyR3 in the SR: evidence for selective stabilization of RyR1 channel. Am. J. Physiol. Cell Physiol. **287**, C36–C45 CrossRef PubMed
13 Voss, A. A., Allen, P. D., Pessah, I. N. and Perez, C. F. (2008) Allosterically coupled calcium and magnesium binding sites are unmasked by ryanodine receptor chimeras. Biochem. Biophys. Res. Commun. **366**, 988–993 CrossRef PubMed
14 Fessenden, J. D., Perez, C. F., Goth, S., Pessah, I. N. and Allen, P. D. (2003) Identification of a key determinant of ryanodine receptor type 1 required for activation by 4-chloro-*m*-cresol. J. Biol. Chem. **278**, 28727–28735 CrossRef PubMed
15 Perez, C. F., Mukherjee, S. and Allen, P. D. (2003) Amino acids 1–1,680 of ryanodine receptor type 1 hold critical determinants of skeletal type for excitation–contraction coupling: role of divergence domain D2. J. Biol. Chem. **278**, 39644–39652 CrossRef PubMed

16 Perez, C. F., Voss, A., Pessah, I. N. and Allen, P. D. (2003) RyR1/RyR3 chimeras reveal that multiple domains of RyR1 are involved in skeletal-type E–C coupling. Biophys. J. **84**, 2655–2663 CrossRef PubMed
17 Wang, Y., Fraefel, C., Protasi, F., Moore, R. A., Fessenden, J. D., Pessah, I. N., DiFrancesco, A., Breakefield, X. and Allen, P. D. (2000) HSV-1 amplicon vectors are a highly efficient gene delivery system for skeletal muscle myoblasts and myotubes. Am. J. Physiol. Cell Physiol. **278**, C619–C626 PubMed
18 Eltit, J. M., Feng, W., Lopez, J. R., Padilla, I. T., Pessah, I. N., Molinski, T. F., Fruen, B. R., Allen, P. D. and Perez, C. F. (2010) Ablation of skeletal muscle triadin impairs FKBP12/RyR1 channel interactions essential for maintaining resting cytoplasmic Ca^{2+}. J. Biol. Chem. **285**, 38453–38462 CrossRef PubMed
19 Huang, Y., Zhou, Y., Castiblanco, A., Yang, W., Brown, E. M. and Yang, J. J. (2009) Multiple Ca^{2+}-binding sites in the extracellular domain of the Ca^{2+}-sensing receptor corresponding to cooperative Ca^{2+} response. Biochemistry **48**, 388–398 CrossRef PubMed
20 Maniccia, A. W., Yang, W., Li, S. Y., Johnson, J. A. and Yang, J. J. (2006) Using protein design to dissect the effect of charged residues on metal binding and protein stability. Biochemistry **45**, 5848–5856 CrossRef PubMed
21 Zhou, Y., Xue, S., Chen, Y. and Yang, J. J. (2013) Probing Ca^{2+}-binding capability of viral proteins with the EF-hand motif by grafting approach. Methods Mol. Biol. **963**, 37–53 CrossRef PubMed
22 Sheridan, D. C., Takekura, H., Franzini-Armstrong, C., Beam, K. G., Allen, P. D. and Perez, C. F. (2006) Bidirectional signaling between calcium channels of skeletal muscle requires multiple direct and indirect interactions. Proc. Natl. Acad. Sci. U.S.A. **103**, 19760–19765 CrossRef PubMed
23 Ogawa, Y., Kurebayashi, N. and Murayama, T. (2000) Putative roles of type 3 ryanodine receptor isoforms (RyR3). Trends Cardiovasc. Med. **10**, 65–70 CrossRef PubMed
24 Ward, C. W., Protasi, F., Castillo, D., Wang, Y., Chen, S. R., Pessah, I. N., Allen, P. D. and Schneider, M. F. (2001) Type 1 and type 3 ryanodine receptors generate different Ca^{2+} release event activity in both intact and permeabilized myotubes. Biophys. J. **81**, 3216–3230 CrossRef PubMed
25 Conklin, M. W., Barone, V., Sorrentino, V. and Coronado, R. (1999) Contribution of ryanodine receptor type 3 to Ca^{2+} sparks in embryonic mouse skeletal muscle. Biophys. J. **77**, 1394–1403 CrossRef PubMed
26 Fessenden, J. D., Wang, Y., Moore, R. A., Chen, S. R., Allen, P. D. and Pessah, I. N. (2000) Divergent functional properties of ryanodine receptor types 1 and 3 expressed in a myogenic cell line. Biophys. J. **79**, 2509–2525 CrossRef PubMed
27 Rossi, D., Simeoni, I., Micheli, M., Bootman, M., Lipp, P., Allen, P. D. and Sorrentino, V. (2002) RyR1 and RyR3 isoforms provide distinct intracellular Ca^{2+} signals in HEK 293 cells. J. Cell Sci. **115**, 2497–2504 PubMed
28 Carroll, A., Yang, W., Ye, Y., Simmons, R. and Yang, J. J. (2006) Amyloid fibril formation by a domain of rat cell adhesion molecule. Cell Biochem. Biophys. **44**, 241–249 CrossRef PubMed
29 Drake, S. K., Lee, K. L. and Falke, J. J. (1996) Tuning the equilibrium ion affinity and selectivity of the EF-hand calcium binding motif: substitutions at the gateway position. Biochemistry **35**, 6697–6705 CrossRef PubMed
30 Horrocks, Jr, W. D. (1993) Luminescence spectroscopy. Methods Enzymol. **226**, 495–538 CrossRef PubMed
31 Lobo, P. A. and Van Petegem, F. (2009) Crystal structures of the N-terminal domains of cardiac and skeletal muscle ryanodine receptors: insights into disease mutations. Structure **17**, 1505–1514 CrossRef PubMed
32 Forsen, S. and Linse, S. (1995) Cooperativity: over the Hill. Trends Biochem. Sci. **20**, 495–497 CrossRef PubMed
33 Richter, M., Schleithoff, L., Deufel, T., Lehmann-Horn, F. and Herrmann-Frank, A. (1997) Functional characterization of a distinct ryanodine receptor mutation in human malignant hyperthermia-susceptible muscle. J. Biol. Chem. **272**, 5256–5260 CrossRef PubMed
34 Murayama, T., Kurebayashi, N., Oba, T., Oyamada, H., Oguchi, K., Sakurai, T. and Ogawa, Y. (2011) Role of amino-terminal half of the S4–S5 linker in type 1 ryanodine receptor (RyR1) channel gating. J. Biol. Chem. **286**, 35571–35577 CrossRef PubMed
35 Yang, T., Ta, T. A., Pessah, I. N. and Allen, P. D. (2003) Functional defects in six ryanodine receptor isoform-1 (RyR1) mutations associated with malignant hyperthermia and their impact on skeletal excitation–contraction coupling. J. Biol. Chem. **278**, 25722–25730 CrossRef PubMed
36 Feng, W., Barrientos, G. C., Cherednichenko, G., Yang, T., Padilla, I. T., Truong, K., Allen, P. D., Lopez, J. R. and Pessah, I. N. (2011) Functional and biochemical properties of ryanodine receptor type 1 channels from heterozygous R163C malignant hyperthermia-susceptible mice. Mol. Pharmacol. **79**, 420–431 CrossRef PubMed
37 Yang, T., Riehl, J., Esteve, E., Matthaei, K. I., Goth, S., Allen, P. D., Pessah, I. N. and Lopez, J. R. (2006) Pharmacologic and functional characterization of malignant hyperthermia in the R163C RyR1 knock-in mouse. Anesthesiology **105**, 1164–1175 CrossRef PubMed
38 Balog, E. M., Fruen, B. R., Shomer, N. H. and Louis, C. F. (2001) Divergent effects of the malignant hyperthermia-susceptible $Arg^{615} \rightarrow Cys$ mutation on the Ca^{2+} and Mg^{2+} dependence of the RyR1. Biophys. J. **81**, 2050–2058 CrossRef PubMed
39 Barrientos, G. C., Feng, W., Truong, K., Matthaei, K. I., Yang, T., Allen, P. D., Lopez, J. R. and Pessah, I. N. (2012) Gene dose influences cellular and calcium channel dysregulation in heterozygous and homozygous T4826I-RYR1 malignant hyperthermia-susceptible muscle. J. Biol. Chem. **287**, 2863–2876 CrossRef PubMed
40 Chugun, A., Sato, O., Takeshima, H. and Ogawa, Y. (2007) Mg^{2+} activates the ryanodine receptor type 2 (RyR2) at intermediate Ca^{2+} concentrations. Am. J. Physiol. Cell Physiol. **292**, C535–C544 CrossRef PubMed
41 Nakai, J., Gao, L., Xu, L., Xin, C., Pasek, D. A. and Meissner, G. (1999) Evidence for a role of C-terminus in Ca^{2+} inactivation of skeletal muscle Ca^{2+} release channel (ryanodine receptor). FEBS Lett. **459**, 154–158 CrossRef PubMed
42 Malmberg, N. J., Varma, S., Jakobsson, E. and Falke, J. J. (2004) Ca^{2+} activation of the cPLA2 C2 domain: ordered binding of two Ca^{2+} ions with positive cooperativity. Biochemistry **43**, 16320–16328 CrossRef PubMed
43 Akke, M., Forsen, S. and Chazin, W. J. (1995) Solution structure of $(Cd^{2+})_1$-calbindin D_{9k} reveals details of the stepwise structural changes along the Apo$\rightarrow(Ca^{2+})_1^{II} \rightarrow (Ca^{2+})_2^{I,II}$ binding pathway. J. Mol. Biol. **252**, 102–121 CrossRef PubMed
44 Kirberger, M., Wang, X., Deng, H., Yang, W., Chen, G. and Yang, J. J. (2008) Statistical analysis of structural characteristics of protein Ca^{2+}-binding sites. J. Biol. Inorg. Chem. **13**, 1169–1181 CrossRef PubMed
45 Treves, S., Scutari, E., Robert, M., Groh, S., Ottolia, M., Prestipino, G., Ronjat, M. and Zorzato, F. (1997) Interaction of S100A1 with the Ca^{2+} release channel (ryanodine receptor) of skeletal muscle. Biochemistry **36**, 11496–11503 CrossRef PubMed
46 Prosser, B. L., Wright, N. T., Hernandez-Ochoa, E. O., Varney, K. M., Liu, Y., Olojo, R. O., Zimmer, D. B., Weber, D. J. and Schneider, M. F. (2008) S100A1 binds to the calmodulin-binding site of ryanodine receptor and modulates skeletal muscle excitation–contraction coupling. J. Biol. Chem. **283**, 5046–5057 CrossRef PubMed
47 Wright, N. T., Prosser, B. L., Varney, K. M., Zimmer, D. B., Schneider, M. F. and Weber, D. J. (2008) S100A1 and calmodulin compete for the same binding site on ryanodine receptor. J. Biol. Chem. **283**, 26676–26683 CrossRef PubMed

Received 25 November 2013/3 March 2014; accepted 18 March 2014
Published as BJ Immediate Publication 18 March 2014, doi:10.1042/BJ20131553

Biochem. J. (2014) **460**, 261–271 (Printed in Great Britain) doi:10.1042/BJ20131553

online data

SUPPLEMENTARY ONLINE DATA

Myoplasmic resting Ca^{2+} regulation by ryanodine receptors is under the control of a novel Ca^{2+}-binding region of the receptor

Yanyi CHEN*[1], Shenghui XUE*[1], Juan ZOU*, Jose R. LOPEZ†, Jenny J. YANG*[2] and Claudio F. PEREZ‡[2]

*Department of Chemistry, Center for Diagnostics and Therapeutics, Georgia State University, 50 Decatur Street, NSC 552, Atlanta, GA 30303, U.S.A.
†Department of Molecular Biosciences, School of Veterinary Medicine, University of California, Davis, 1089 Veterinary Medicine Drive, Davis, CA 95616, U.S.A.
‡Department of Anesthesiology, Perioperative and Pain Medicine, Brigham and Women's Hospital, Harvard Medical School, 20 Shattuck Street, Boston, MA 02115, U.S.A.

SUPPLEMENTARY METHODS

Tryptophan and Tb^{3+} fluorescence spectroscopy

Ca^{2+}-induced fluorescence changes of CLR-1 or CLR-3 (2 μM) were monitored in the presence of 10 mM Pipes (pH 6.8) and 100 mM KCl. All solutions were dialysed against Chelex-100 for at least 24 h to remove contaminant cations. Intrinsic tryptophan fluorescence was monitored using excitation at 280 nm and emission between 300 and 400 nm with 2–4-nm band passes. Ca^{2+} dissociation constants of the CLR domains were calculated separately for each binding phase. The first binding phase was fitted to eqn (S1):

$$f = \frac{([P]_T + [M]_T + K_{d1}) - \sqrt{([P]_T + [M]_T + K_{d1})^2 - 4\,[P]_T\,[M]_T}}{2\,[P]_T} \quad \text{(S1)}$$

where f is the fractional change, K_{d1} is the dissociation constant, and $[P]_T$ and $[M]_T$ are the total concentration of protein and Ca^{2+} respectively. The second co-operative Ca^{2+}-binding phase was fitted to eqn (S2):

$$\Delta S = \Delta S_1 + \Delta S_2 \frac{[M]^h}{K_{d2}^h + [M]^h} \quad \text{(S2)}$$

where ΔS is the total fluorescence signal change, ΔS_1 and ΔS_2 are the signal changes in the first and second binding phases respectively, [M] is the Ca^{2+} concentration, h is the Hill coefficient, and K_{d2} is the Ca^{2+} dissociation constant for the second binding phase.

Tb^{3+}-binding affinity of CLR-1 and CLR-3 was obtained by Tb^{3+} FRET analysis as described previously [1,2]. Briefly, 2 μM purified CLR-1 or CLR-3 was resuspended in binding solution (10 mM Pipes, pH 6.8, and 100 mM KCl) and titrated with increasing concentrations of $TbCl_3$. FRET was then acquired by excitation of tryptophan (donor) at 280 nm and collection of Tb^{3+} fluorescence emission (acceptor) between 500 and 600 nm using a glass filter to cut off emission below 400 nm. Specific changes in Tb^{3+} fluorescent signal were obtained from the emission intensity at 545 nm after removal of free Tb^{3+} background signal. The Tb^{3+} dissociation constant for CLR-1 or CLR-3 was obtained by fitting the normalized fluorescent intensity data to eqn (S3):

$$f = \frac{([P]_T + [M]_T + K_d) - \sqrt{([P]_T + [M]_T + K_d)^2 - 4\,[P]_T\,[M]_T}}{2\,[P]_T} \quad \text{(S3)}$$

where f is the fractional change, K_d is the dissociation constant, and $[P]_T$ and $[M]_T$ are the total concentration of protein and Tb^{3+} respectively.

Cell membrane isolation and immunoblotting

Crude membrane preparations were made from three 10-cm-diameter plates of 5-day differentiated dyspedic myotubes 36 h after infection with $(1.5–2) \times 10^6$ virion particles. Myotubes were harvested in PBS and centrifuged at 250 ***g*** for 10 min. Cell pellets were resuspended in buffer consisting of 250 mM sucrose and 10 mM Hepes (pH 7.4), supplemented with 1 mM EDTA, 10 μg/ml leupeptin, 0.7 μg/ml pepstatin A, 5 μg/ml aprotinin and 0.1 mM Pefabloc SC and then homogenized using a Tissue-Tearor™ cell disrupter (Biospect Products). Whole-cell homogenates were centrifuged at 1500 ***g*** for 20 min and the supernatants then collected and recentrifuged at 100 000 ***g*** for 60 min at 4 °C. Membrane pellets were finally resuspended in 250 mM sucrose and 20 mM Hepes (pH 7.4), quick frozen in liquid N_2 and stored at −80 °C. Proteins (25–30 μg/lane) were separated in discontinuous SDS/PAGE 7–12 % or 7–15 % gels [3,4] and then electroblotted on to PVDF membranes for 90 min at 50 V. Membrane sections containing the protein to be tested were then excised and immunoblotted separately with monoclonal antibody 34C (J. Airey and J. Sutko, DSHB (Developmental Study Hybridoma Bank), University of Iowa, Iowa City, IA, U.S.A.), which recognizes both RyR1 and RyR3, monoclonal anti-calsequestrin-1 (MA3-913, Thermo Scientific), monoclonal anti-SERCA1 (MA3-911,Thermo Scientific) or polyclonal anti-GAPDH (glyceraldehyde-3-phosphate dehydrogenase) (FL-335 from Santa Cruz Biotechnology) antibodies. Membranes were then incubated with either goat anti-mouse or goat anti-rabbit horseradish-peroxidase-conjugated secondary antibody and developed with SuperSignal ultra chemiluminescent substrate (Pierce) and the intensity of the signal was collected using a Kodak Imaging Station 4000MM PRO (Carestream Health). Band densitometry of the identified proteins was performed using Kodak MI Software (version 4.5.1 ES). For each blot net band intensities were normalized to GAPDH expression to correct for protein loading and expressed as the fraction of the corresponding band of RyR1-expressing myotubes.

Data analysis

Statistical differences among datasets were evaluated using one-way Kruskal–Wallace ANOVA (non-parametric) analysis using Prism 5.0 (GraphPad Software). Unless indicated otherwise, results are means ± S.D.

[1] These authors contributed equally to this work.
[2] Correspondence may be addressed to either of these authors (email jenny@gsu.edu or cperez@zeus.bwh.harvard.edu).

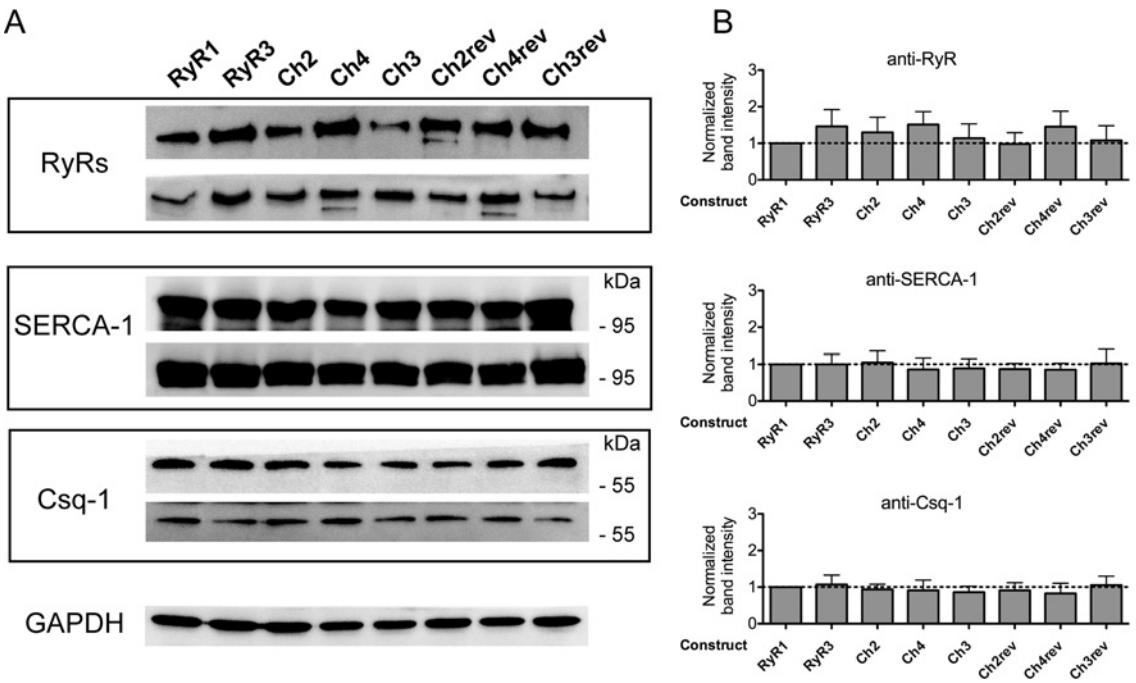

Figure S1 Relative expression of chimaeric RyRs in dyspedic myotubes

(**A**) Western blot analysis of crude membrane homogenates showing relative expression levels of RyRs, SERCA1 and calsequestrin-1 (Csq-1) of dyspedic myotubes infected with the wild-type or chimaeric constructs shown in Figure 1(A) of the main text. For each immunoblot, representative results of two different membrane homogenates are shown to highlight intrinsic variability between preparations. (**B**) Mean ± S.D. band intensity for each protein expressed as a fraction of the RyR1-expressing lane (broken line) for four to five blots from two separated membrane preparations. ANOVA one-way analysis of variance (Tukey's multiple comparison test) detected not statistically significant differences in band intensity among the different constructs.

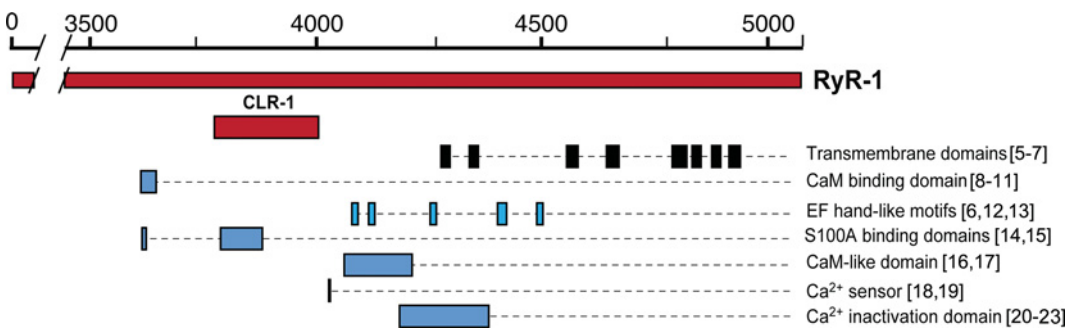

Figure S2 Localization of Ca^{2+}-binding/regulatory regions of RyR1

Mapping of the CLR-1 region within the context of the C-terminal tail of RyR1. Boxes represent the location of various domains of RyR1 reported to be involved in Ca^{2+}-binding or Ca^{2+}-mediated regulation. The location of CLR-1 does not appear to coincide with any of the prospective Ca^{2+}-binding regions currently identified in RyR1.

REFERENCES

1 Maniccia, A. W., Yang, W., Li, S. Y., Johnson, J. A. and Yang, J. J. (2006) Using protein design to dissect the effect of charged residues on metal binding and protein stability. Biochemistry **45**, 5848–5856 CrossRef PubMed

2 Zhou, Y., Xue, S., Chen, Y. and Yang, J. J. (2013) Probing Ca^{2+}-binding capability of viral proteins with the EF-hand motif by grafting approach. Methods Mol. Biol. **963**, 37–53 CrossRef PubMed

3 Laemmli, U. K. (1970) Cleavage of structural proteins during the assembly of the head of bacteriophage T4. Nature **227**, 680–685 CrossRef PubMed

4 King, Jr, L. E. and Morrison, M. (1976) The visualization of human erythrocyte membrane proteins and glycoproteins in SDS polyacrylamide gels employing a single staining procedure. Anal. Biochem. **71**, 223–230 CrossRef PubMed

5 Grunwald, R. and Meissner, G. (1995) Lumenal sites and C terminus accessibility of the skeletal muscle calcium release channel (ryanodine receptor). J. Biol. Chem. **270**, 11338–11347 CrossRef PubMed

6 Takeshima, H., Nishimura, S., Matsumoto, T., Ishida, H., Kangawa, K., Minamino, N., Matsuo, H., Ueda, M., Hanaoka, M., Hirose, T. et al. (1989) Primary structure and expression from complementary DNA of skeletal muscle ryanodine receptor. Nature **339**, 439–445 CrossRef PubMed

7 Zorzato, F., Fujii, J., Otsu, K., Phillips, M., Green, N. M., Lai, F. A., Meissner, G. and MacLennan, D. H. (1990) Molecular cloning of cDNA encoding human and rabbit forms of the Ca^{2+} release channel (ryanodine receptor) of skeletal muscle sarcoplasmic reticulum. J. Biol. Chem. **265**, 2244–2256 PubMed

8 Chen, S. R. and MacLennan, D. H. (1994) Identification of calmodulin-, Ca^{2+}-, and ruthenium red-binding domains in the Ca2 + release channel (ryanodine receptor) of rabbit skeletal muscle sarcoplasmic reticulum. J. Biol. Chem. **269**, 22698–22704 PubMed

9 Menegazzi, P., Larini, F., Treves, S., Guerrini, R., Quadroni, M. and Zorzato, F. (1994) Identification and characterization of three calmodulin binding sites of the skeletal muscle ryanodine receptor. Biochemistry **33**, 9078–9084 CrossRef PubMed

10 Rodney, G. G., Krol, J., Williams, B., Beckingham, K. and Hamilton, S. L. (2001) The carboxy-terminal calcium binding sites of calmodulin control calmodulin's switch from an activator to an inhibitor of RYR1. Biochemistry **40**, 12430–12435 CrossRef PubMed
11 Yamaguchi, N., Xin, C. and Meissner, G. (2001) Identification of apocalmodulin and Ca^{2+}-calmodulin regulatory domain in skeletal muscle Ca^{2+} release channel, ryanodine receptor. J. Biol. Chem. **276**, 22579–22585 CrossRef PubMed
12 Hamada, T., Sakube, Y., Ahnn, J., Kim, D. H. and Kagawa, H. (2002) Molecular dissection, tissue localization and Ca^{2+} binding of the ryanodine receptor of *Caenorhabditis elegans*. J. Mol. Biol. **324**, 123–135 CrossRef PubMed
13 Xiong, H., Feng, X., Gao, L., Xu, L., Pasek, D. A., Seok, J. H. and Meissner, G. (1998) Identification of a two EF-hand Ca^{2+} binding domain in lobster skeletal muscle ryanodine receptor/Ca^{2+} release channel. Biochemistry **37**, 4804–4814 CrossRef PubMed
14 Treves, S., Scutari, E., Robert, M., Groh, S., Ottolia, M., Prestipino, G., Ronjat, M. and Zorzato, F. (1997) Interaction of S100A1 with the Ca^{2+} release channel (ryanodine receptor) of skeletal muscle. Biochemistry **36**, 11496–11503 CrossRef PubMed
15 Wright, N. T., Prosser, B. L., Varney, K. M., Zimmer, D. B., Schneider, M. F. and Weber, D. J. (2008) S100A1 and calmodulin compete for the same binding site on ryanodine receptor. J. Biol. Chem. **283**, 26676–26683 CrossRef PubMed
16 Gangopadhyay, J. P. and Ikemoto, N. (2006) Role of the Met^{3534}–Ala^{4271} region of the ryanodine receptor in the regulation of Ca^{2+} release induced by calmodulin binding domain peptide. Biophys. J. **90**, 2015–2026 CrossRef PubMed
17 Xiong, L., Zhang, J. Z., He, R. and Hamilton, S. L. (2006) A Ca^{2+}-binding domain in RyR1 that interacts with the calmodulin binding site and modulates channel activity. Biophys. J. **90**, 173–182 CrossRef PubMed
18 Chen, S. R., Ebisawa, K., Li, X. and Zhang, L. (1998) Molecular identification of the ryanodine receptor Ca^{2+} sensor. J. Biol. Chem. **273**, 14675–14678 CrossRef PubMed
19 Li, P. and Chen, S. R. (2001) Molecular basis of Ca^{2+} activation of the mouse cardiac Ca^{2+} release channel (ryanodine receptor). J. Gen. Physiol. **118**, 33–44 CrossRef PubMed
20 Bhat, M. B., Zhao, J., Takeshima, H. and Ma, J. (1997) Functional calcium release channel formed by the carboxyl-terminal portion of ryanodine receptor. Biophys. J. **73**, 1329–1336 CrossRef PubMed
21 Chen, S. R., Zhang, L. and MacLennan, D. H. (1992) Characterization of a Ca^{2+} binding and regulatory site in the Ca^{2+} release channel (ryanodine receptor) of rabbit skeletal muscle sarcoplasmic reticulum. J. Biol. Chem. **267**, 23318–23326 PubMed
22 Du, G. G., Khanna, V. K. and MacLennan, D. H. (2000) Mutation of divergent region 1 alters caffeine and Ca^{2+} sensitivity of the skeletal muscle Ca^{2+} release channel (ryanodine receptor). J. Biol. Chem. **275**, 11778–11783 CrossRef PubMed
23 Du, G. G. and MacLennan, D. H. (1999) Ca^{2+} inactivation sites are located in the COOH-terminal quarter of recombinant rabbit skeletal muscle Ca^{2+} release channels (ryanodine receptors). J. Biol. Chem. **274**, 26120–26126 CrossRef PubMed

Received 25 November 2013/3 March 2014; accepted 18 March 2014
Published as BJ Immediate Publication 18 March 2014, doi:10.1042/BJ20131553